

Autonomous Interactive Correction MLLM for Robust Robotic Manipulation

Chuyan Xiong^{1,2*} Chengyu Shen^{1*} Xiaoqi Li^{1*} Kaichen Zhou^{1†}
Jiaming Liu¹ Ruiping Wang² Hao Dong^{1‡}

¹School of Computer Science, Peking University

²Institute of Computing Technology, Chinese Academy of Sciences

Abstract: The ability to reflect on and correct failures is crucial for robotic systems to interact stably with real-life objects. Observing the generalization and reasoning capabilities of Multimodal Large Language Models (MLLMs), previous approaches have aimed to utilize these models to enhance robotic systems accordingly. However, these methods typically focus on high-level planning corrections using an additional MLLM, with limited utilization of failed samples to correct low-level contact poses. To address this gap, we propose an Autonomous Interactive Correction (AIC) MLLM, which makes use of previous low-level interaction experiences to correct SE(3) pose predictions. Specifically, AIC MLLM is initially fine-tuned to acquire both pose prediction and feedback prompt comprehension abilities. We carefully design two types of prompt instructions through interactions with objects: **1)** visual masks to highlight unmovable parts for position correction, and **2)** textual descriptions to indicate potential directions for rotation correction. During inference, a Feedback Information Extraction module is introduced to recognize the failure cause, allowing AIC MLLM to adaptively correct the pose prediction using the corresponding prompts. To further enhance manipulation stability, we devise a Test Time Adaptation strategy that enables AIC MLLM to better adapt to the current scene configuration. Finally, extensive experiments are conducted in both simulated and real-world environments to evaluate the proposed method. The results demonstrate that our AIC MLLM can efficiently correct failure samples by leveraging interaction experience prompts. Real-world demonstration can be found at <https://sites.google.com/view/aic-mlm>

Keywords: Robot Manipulation, Large Language Model, Failure Correction

1 Introduction

Developing a versatile robot has always been a primary goal for researchers in embodied artificial intelligence. Despite numerous generalization strategies proposed [1, 2, 3, 4], failures remain inevitable due to the complexity of real-world environments. Therefore, beyond directly enhancing the robot’s generalization ability, it is also crucial to enable the robot to reflect on and correct its failure actions.

In recent years, the powerful common-sense generalization and reasoning abilities of Multimodal Large Language Models (MLLMs) [5, 6, 7, 8, 9, 10] have attracted the attention of robotic researchers. These capabilities make MLLMs and LLMs naturally suited for understanding, analyzing, explaining failures, and even making corrections based on them. REFLECT [11] innovatively summarizes hierarchical sensor information and inputs it into an LLM in textual form to obtain explanations for errors. Additionally, other works [12, 13, 14, 15, 16, 17, 18, 19] are also exploring the ways and capabilities of LLMs in handling errors in the field of robotics.

* Equal contribution: chuyan.xiong@vipl.ict.ac.cn, 912074188@stu.xjtu.edu.cn, clorisli@stu.pku.edu.cn

† Project leader: kc.zhou2020@hotmail.com

‡ Corresponding author: hao.dong@pku.edu.cn

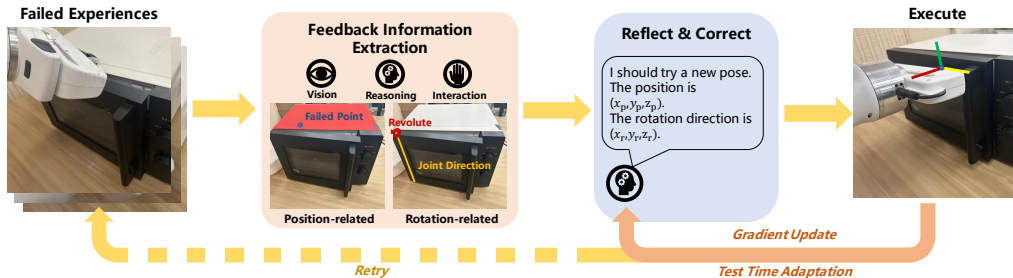


Figure 1: **Correction process of AIC MLLM.** Given a failed interaction, we first extract feedback information regarding the object’s geometry, then enable the model to reflect and correct both position and rotation estimation, thereby generating a more accurate SE(3) pose.

While these works can reflect and correct high-level tasks, such as task planning, they still struggle to correct low-level SE(3) pose actions. For example, even if a robot recognizes that it failed to open a microwave to place food inside, it may still encounter difficulty in selecting the correct contact pose, ultimately resulting in task failure. In such cases, previous methods cannot automatically recover from these errors. Given that learning from failed scenarios is an inherent capability of humans, our goal is to imbue the agent with a similar capacity. By utilizing failed attempts, we seek to enhance its ability to comprehend geometry and, consequently, improve its generation of low-level actions.

Leveraging this insight, we propose an Autonomous Interactive Correction (AIC) MLLM, which leverages previous low-level interaction experiences to correct manipulation SE(3) poses. First, we fine-tune a pre-trained MLLM to enable it not only to predict manipulation poses but also to understand the instructions provided by the feedback information extraction system and reflect on them for correction. To realize this goal, we carefully design two types of prompt instructions to assist the MLLM in failure correction, including position and rotation prompts. Specifically, we create visual masks to highlight unmovable parts for position correction and use textual descriptions to indicate potential manipulation directions for rotation correction. During inference, the model initially performs pose prediction. If an error occurs, the Feedback Information Extraction module is introduced to detect the cause of failure, enabling the AIC MLLM to adaptively correct the end-effector pose prediction using the corresponding prompts. To further enhance manipulation stability, we devise a Test Time Adaptation strategy for AIC MLLM. This allows our model to iteratively update itself during inference and adapt to the current scene configuration. With our proposed AIC MLLM, the robot can efficiently improve its manipulation stability through interactive attempts in any scenario, especially for unseen categories during training.

The main contributions of this paper could be summarized as follow: 1) We introduce AIC MLLM, a framework that utilizes MLLM for correcting SE(3) pos predictions by learning from low-level interaction failures. 2) We design visual and textual prompts to guide position and rotation corrections, and incorporate a feedback information extraction module to adaptively correct pose predictions based on identified failure causes. 3) We implement a test-time adaptation module to enhance manipulation stability, with extensive experiments demonstrating the efficacy of AIC MLLM in both simulated and real-world environments.

2 Related Work

Robotic Failure Correction. As Multimodal Large Language Models (MLLMs) advance, robot correction mechanisms have garnered increasing attention. These works fall into two main categories: human-guided correction and self-correction. the former approaches[16, 15, 13] like YAY robot[16] and DROC[15] utilize human feedback to adjust robot behavior. Conversely, self-reflective methods[17, 12, 11, 14, 18, 19] such as inner monologue[12] and REFLECT[11] enable robots to learn from errors and correct autonomously. We focus on the latter type, aiming to develop a system capable of automatic self-reflection and correction at low-level pose stage.

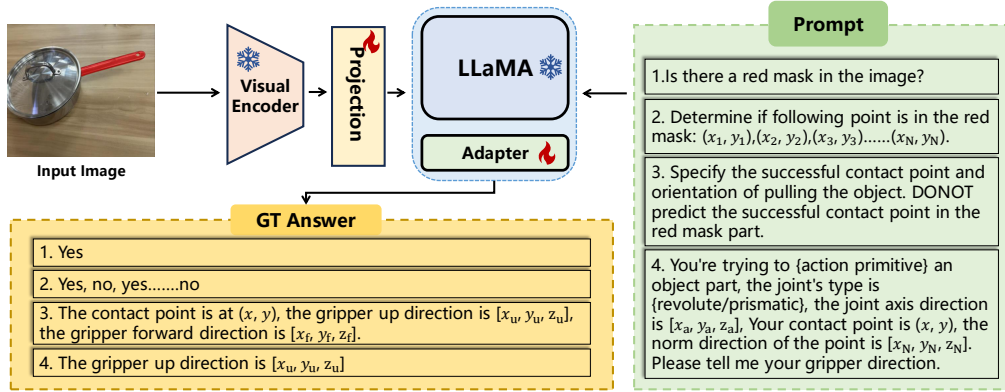


Figure 2: **Training of AIC MLLM.** We gradually enable the model to predict poses and comprehend both visual and linguistic feedback prompts including object parts and axis information.

MLLMs with Prompt Instruction. The performance of MLLMs heavily depends on input prompts. With the integration of diverse input modalities, prompt instructions have become essential for MLLMs to perform specific tasks [20, 21]. Some researches focus on image labeling and annotating coordinates as prompts [22, 23]. Vip-llava [21] and SPHINX-V [20] have been trained to understand visual prompts. In this paper, we use visual prompts and textual prompts to indicate unmovable parts and potential directions for manipulation.

Robotic Manipulation with MLLMs. MLLMs have also been applied to robotic manipulation [24, 25, 26, 27, 28], with models such as Palm-e [24], Voxposer [25], RT-2 [27], and ManipLLM [28] showing promise for high-level planning, mid-level cost function injection, and direct low-level pose output. While high-level correction has been widely studied, low-level correction remains largely unexplored. Due to space limitations, we provide additional related work in the Appendix.

3 Method

3.1 Framework Overview

During training (3.2), we enable the model to predict poses, and comprehend given feedback prompts, such as visual masks highlighting unmovable part or text describing axis information, and correct the pose prediction accordingly. During testing, if the model’s interaction with the object results in failure, we use an **Feedback Information Extraction (FIE)** module to obtain error information related to the geometry articulated object (3.3.1). This error information is then fed back into the trained model, allowing it to reflect on the failure’s cause and predict a new SE(3) pose for interacting with the object, aiming to achieve successful manipulation (3.3.2). To enable the model to better adapt to the current testing configuration, we devise a Test Time Adaptation (TTA) strategy. This strategy allows the model to learn from the ongoing sample and improve its ability to handle upcoming samples (3.3.3).

3.2 Training Phase

In this section, we introduce how we train our model capable of both executing manipulation tasks and correcting failure interaction based on feedback. To achieve this goal, we first enable our model to output the manipulation pose which contains both position and rotation, enabling interaction with the object. Next, to enable our model to correct failure interaction based on feedback, we have constructed two prompt interfaces: a visual mask prompt and linguistic prompts. These interfaces convey part positional and rotational information of the object, extracted from failure samples, to the model. This enables the model to generate new predictions based on this prior knowledge.

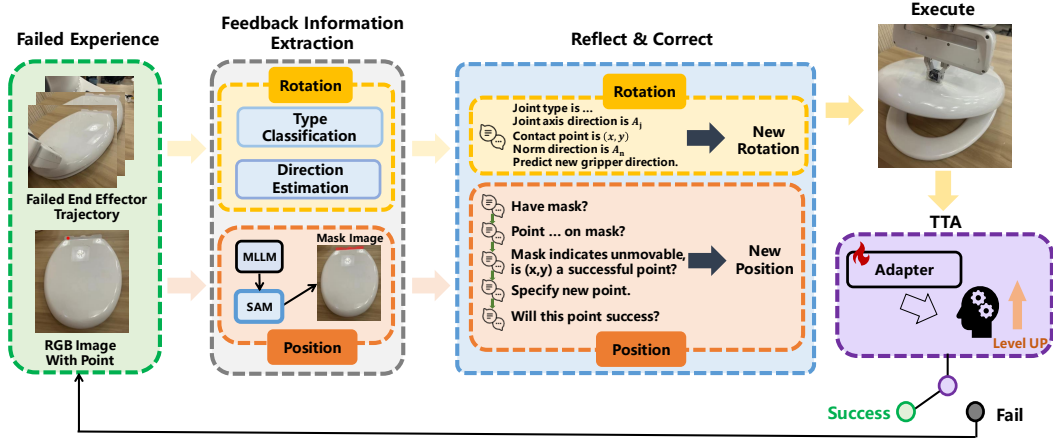


Figure 3: **Testing of AIC MLLM.** If failure interaction occurs, an FIE module is utilized to extract feedback information from previous failure attempts. This feedback information is integrated into visual and linguistic prompts, which are then fed into the trained model, enabling it to reflect, correct, and generate new action predictions. After inference on each test sample, the model undergoes parameter updates in the TTA module to enhance generalization to the current testing configuration.

3.2.1 Postional Error Interface

Based on our observations, if the model predicts points on unmovable parts, no method can successfully manipulate these parts. Therefore, to prevent the model from making invalid interactions on unmovable parts, we summarize these positional error information by segmenting out unmovable part, and enable our model to comprehend it.

Specifically, we denote a part of the articulated object as unmovable by applying a red-colored mask. We then ensure that our model comprehends the red mask on image and avoid from predicting on unmovable parts through progressively training with the following three VQA tasks:

(1) **Mask Image Classification** To ensure that our model understands that parts labeled with a red mask are unmovable, we first need to train it to recognize whether there is a mask in the image. Specifically, we obtain the location of unmovable part in simulator and add red mask on it. Then, as shown in the first prompt in Fig.7, we prompt the model to answer the first question "Is there a red mask in the image?" based on the input masked image. For the ground truth answer, we just use "Yes" and "No", which is supervised under cross-entropy loss \mathcal{L}_H .

(2) **Mask Position Reasoning** After the model understands what a mask is, we also need it to understand where the mask is located. We randomly select N pixel points $(x_1, y_1) \dots (x_N, y_N)$ and ask the model to identify whether each point is on the mask. As shown in the second prompt on Fig.7, we format the text prompt with corresponding answer of "Yes" and "No" based on the actual ground truth mask, determining whether each point is on the mask or not. This task is supervised under cross-entropy loss \mathcal{L}_P .

(3) **Correct Based On Mask** In the third prompt of Fig.7, once the model comprehends the mask and its location, we prompt it to predict a new pose based on the constraint of unmovable part. Given that MLLM are good at handling discretized data, we discretize the direction vectors into 100 bins, with each bin spanning 0.02. This task is supervised under cross-entropy loss \mathcal{L}_C .

3.2.2 Rotational Error Interface

The information related to position only affects the correction of the contact point position, whereas the correction of pose also requires correction of the gripper direction. For articulated objects, the most crucial information for determining a valid gripper direction is the type and direction of the joint. For articulated objects, there are mainly two types of joints: prismatic and revolute. We observe that often, even when the part of the articulated object fails to reach the expected state, it still exhibits some degree of movement. For instance, when a robotic arm attempts to open a door but

fails to fully complete it, external forces may still cause the door to move to some extent. Therefore, we utilize the movement in this interaction to capture information about the type of joint and the axis direction, enabling the model to reflect on and correct its actions based accordingly.

Specifically, as shown in the last prompt in Fig 7, we incorporate the joint type information and direction information into the text prompt, modeling it as a VQA task. The model is required to provide new direction predictions based on joint information, the current contact point, and the current normal direction, which can also provide some hints for predicting a valid contact direction. This task is supervised under cross-entropy loss \mathcal{L}_R . Note that, in simulator, we can obtain the accurate joint type, joint axis direction and norm direction, and calculate the actual movement direction of the part. However, in real-world scenarios, the estimated joint axis direction may not be accurate and can be noisy. To mitigate error accumulation, we introduce noise into the training process by adding a random rotation between -20° and 20° around the obtained axis direction. This approach enhances the robustness of the model’s predictions based on these priors.

We jointly train the four tasks under the objective $\mathcal{L} = \mathcal{L}_H + \mathcal{L}_P + \mathcal{L}_C + \mathcal{L}_R$

3.3 Testing Phase

We introduce the process of our framework during the testing phase. Specifically, given an object image, the model predicts the 2D contact point and the SE(3) rotation. The contact point is subsequently transformed into 3D coordinates using a depth map, facilitating the initial interaction with the object. If the interaction results in failure, we use an FIE module(3.3.1) to extract feedback information from previous failure attempt. This feedback information is then incorporated into the visual and linguistic prompts, which are fed into the trained model, allowing the model to reflect and correct, and thereby generating new action predictions(3.3.2). Additionally, after inference on each test sample, the model undergoes parameter updates in the TTA module(3.3.3) to better generalize to the current testing configuration. The complete prompts in Fig. 3 are shown in supplement material.

3.3.1 Feedback Information Extraction (FIE)

In real-world scenarios, we cannot directly obtain the leveraged reflect information as that in simulator. Therefore, we extract feedback information related to position and rotation based on the previous failure attempt.

Position-related Information Extraction During the interaction process, our objective is to determine if the predicted contact point lies on unmovable part. If so, our aim is to pinpoint the unmovable part’s location and prevent from any subsequent operations on it. Specifically, we first employ the off-the-shelf VIP-LLaVA [29] to confirm whether it is unmovable. This model allows users to mark images with visual prompts, *i.e.*, a dot on the image, and interact with the model using language queries. Therefore, we draw the predicted contact point as a red dot on the object. Then, as shown in Fig. 3, we input the drawn image along with the textual prompt to VIP-LLaVA, obtaining its response to determine whether the part is movable or not. If contact point is on unmovable part, we then use SAM [30] to perform hierarchical segmentation with the red dot as the prompt, and among them, we select the smallest mask to represent the segmentation of the unmovable part. Note that multiple failed interactions with an object may occur, and the information about unmovable parts generated from each interaction will accumulate as multiple red masks on the object.

Rotation-related Information Extraction Our goal is to obtain joint type and axis direction based on the history interaction attempt. When interaction with the object, *e.g.*, when pulling a door, we can determine the trajectory of the end effector. If the trajectory is a straight line, we classify it as a prismatic axis. Conversely, if the trajectory is of an arc shape, we classify it as a revolute axis. To determine the axis direction, for prismatic axis, we consider the axis direction to be the same as its direction of movement. For a revolute axis, even if the interaction fails, as long as the end effector moves, we can determine the axis direction from the end effector’s trajectory. Specifically, if there is only one failed interaction, we select the start position p_s^1 , end position p_e^1 , and midpoint p_m^1 of the trajectory, all belonging to \mathbb{R}^3 , forming two directional vectors $\frac{p_s^1 - p_m^1}{\|p_s^1 - p_m^1\|}$ and $\frac{p_m^1 - p_e^1}{\|p_m^1 - p_e^1\|}$. The cross product

of these two vectors yields the axis direction: $\vec{A} = \overrightarrow{p_s^1 p_m^1} \times \overrightarrow{p_m^1 p_e^1}$. If there are multiple n failed interactions with movement, we use the end effector’s movement vectors from these interactions to perform cross products, providing a more accurate axis direction: $\vec{A} = \overrightarrow{p_s^1 p_e^1} \times \dots \overrightarrow{p_s^n p_e^n}$.

3.3.2 Model Inference

After extracting feedback information from the failed experiences, the trained model should reflect and correct itself. Since the failure can be attributed to either an invalid position or direction, we first need to determine which of these factors caused the failure and then make corrections accordingly. Specifically, a failure interaction can result in either movement or no movement. In cases of the former, it indicates that the contact point is on a movable part and can cause movement. Therefore, we consider this a valid contact point and focus on rotation correction. For the latter cause, we utilize the normal direction to interact with the object, which usually results in slight movements if the position is movable. If even the normal direction fails to induce movement, we then assume that position correction is necessary.

Position Correction. After determine position needs to be corrected, we employ chain-of-thought [31] to guide the model understand feedback, *i.e.*, visual mask prompts and generate new contact point to prevent from predicting on unmovable part. As shown in Fig 3, the first two steps are consistent with the training phase steps. In the third step, we prompt the model to determine whether the previously predicted points are on unmovable parts, compelling it to reflect on the reason behind the previous failures. Next, in the fourth step, we request the model to output a new SE(3) pose based on the reflection. Finally, in the fifth step, we ask the model to evaluate whether the newly predicted pose will result in a successful interaction, reinforcing its ability to reflect on the outcome.

Rotation Correction If rotation correction is necessary, as shown in Fig.3, we adopt the same direction correction process as in the training phase. We directly perform direction correction using the error information obtained from FIE with text prompts guidance. During this process, the contact point remains fixed and the model will output a new gripper direction.

















3.3.3 Test Time Adaptation(TTA)















To enable the continuous evolution of the model and allow it to rapidly adapt to the current configuration, we propose the Test Time Adaptation (TTA) strategy. During TTA, the model updates itself after each sample inference to learn from the sample it has just processed. The updated model then infers on the next sample, updates again, and this model updating continues. Specifically, we use model π_{t-1} at timestamp $t - 1$ to inference on test sample at timestamp t . The model can **only** utilize the attempts made on the sample at timestamp t to update itself to π_t , thus enhancing its performance when dealing with subsequent samples under the same testing configuration.

The input-ground truth pairs used to update the model are as follows: To start with, since we can obtain the ground truth for the first two steps in Fig. 7 whether there is a red mask on the image and identifying its location—we update the model with these position-related question answer pairs. This enables the model to recognize which parts of the object are unmovable, thereby avoiding predictions on those parts. In addition, we also want the model to improve its manipulation ability by learning from successful correction experiences. Therefore, for poses that result in successful manipulation after correction, we use the fourth step of Fig. 7 to update the model, with the corrected pose serving as the ground truth.

We use cross-entropy as the supervision signal to update the model. Additionally, to prevent the model from forgetting the knowledge acquired during the training phase, we gradually decrease the learning rate as the number of test samples increases.

Table 1: Comparisons with baseline methods and ablation study.

Method	Train Categories															
																
UMPNet [32]	0.23	0.36	0.41	0.22	0.24	0.30	0.43	0.34	0.51	0.21	0.66	0.27	0.23	0.23	0.29	0.60
FlowBot3D [33]	0.45	0.48	0.45	0.32	0.32	0.37	0.43	0.23	0.26	0.14	0.39	0.31	0.38	0.32	0.23	0.43
ManipLLM [28]	0.72	0.56	0.32	0.79	0.48	0.53	0.66	0.69	0.39	0.52	0.53	0.4	0.64	0.73	0.62	0.52
base model	0.21	0.51	0.25	0.52	0.10	0.40	0.30	0.31	0.50	0.29	1.00	0.79	0.13	0.56	0.23	0.80
Ours-w/o pretrain	0.31	0.66	0.67	0.66	0.95	0.60	0.68	0.46	0.50	0.43	1.00	0.81	0.45	0.66	0.38	0.74
Ours-w/o pos	0.76	0.66	0.67	0.84	0.76	0.53	0.59	0.54	0.31	0.57	0.67	0.81	0.34	0.76	0.31	0.93
Ours-w/o rot	0.81	0.68	0.67	0.83	0.86	0.53	0.54	0.62	0.38	0.68	0.67	0.84	0.34	0.73	0.31	0.93
Ours-w/o tta	0.86	0.73	0.50	0.25	0.81	0.80	0.68	0.62	0.38	0.68	1.00	0.86	0.55	0.83	0.38	0.93
Ours	0.86	0.73	0.58	0.84	0.81	0.80	0.73	0.65	0.50	0.79	0.67	0.84	0.60	0.86	0.54	1.00

Method	Train Categories					Test Categories											
					AVG											AVG	
UMPNet [32]	0.32	0.30	0.11	0.58	0.34	0.36	0.36	0.38	0.47	0.21	0.12	0.24	0.23	0.28	0.12	0.28	
FlowBot3D [33]	0.19	0.33	0.23	0.47	0.33	0.29	0.47	0.64	0.31	0.27	0.30	0.09	0.41	0.35	0.37	0.35	
ManipLLM [28]	0.39	0.75	0.44	0.67	0.57	0.32	0.22	0.65	0.69	0.38	0.85	0.27	0.53	0.26	0.38	0.47	
base model	0.00	0.42	0.13	0.60	0.40	0.09	0.10	0.68	0.17	0.50	0.56	0.13	0.27	0.04	0.38	0.34	
Ours-w/o pretrain	0.00	0.63	0.16	1.00	0.57	0.27	0.10	0.75	0.67	0.43	0.73	0.30	0.46	0.16	0.75	0.45	
Ours-w/o pos	0.60	0.64	0.15	1.00	0.61	0.27	0.35	0.71	0.50	0.57	0.77	0.65	0.61	0.24	0.63	0.54	
Ours-w/o rot	0.60	0.67	0.15	1.00	0.63	0.36	0.33	0.68	0.67	0.64	0.78	0.61	0.61	0.21	0.63	0.53	
Ours-w/o tta	0.60	0.70	0.27	1.00	0.69	0.36	0.45	0.76	0.83	0.64	0.86	0.70	0.78	0.64	0.69	0.68	
Ours	0.60	0.69	0.34	1.00	0.72	0.55	0.56	0.77	0.67	0.50	0.86	0.78	0.80	0.56	0.69	0.70	

4 Experimental Results

4.1 Experiment Setting

Implementation Details. We use SAPIEN [34] and the PartNet-Mobility [35] dataset to set up the experiment environment. We employ a Franka Panda on-the-fly suction gripper to execute the end-effector actions. We randomly sample about 12K successful manipulation samples across 20 categories to build dataset D_o . Specifically, we randomly sample the contact points and the gripper directions, then determine if the interaction is successful. If it is, we save the data; otherwise, we delete it. We sample both pulling and pushing action primitives. After that, we augment D_o by supplementing each example with the necessary training information, such as mask, joint direction, joint type, etc., thus obtaining D_{aug} which is used to train our model. For testing, we also sample about 1K successful manipulation samples across 30 categories to ensure the objects can be manipulated. Follow the work before[28], we only evaluate the pulling action primitives. We finetuned LLaMA-Adapter [36] on an 80G A800 GPU for 4 epochs. Each epoch takes about 1 hour. Specifically, it uses a pre-trained CLIP [37] as the visual encoder, a 7B LLaMA [38] as the language model, and a multi-modal projection module with 32 transformer layers as the alignment bridge.

Evaluation Metrics. We adopt the manipulation success rate to measure performance, which is the ratio of the number of successful samples to the total number of all test samples. For the definition of success in pulling, we require a difference of more than 0.01 units between the initial and final object poses or 0.5 relative to the total motion range of the articulated part, and we also require the dot product of the predicted gripper direction and the actual movement direction of the object to be greater than 0.3.

Baseline & Ablation Setting. (1) UMPNet, FlowBot3D: two expert suction manipulation models that use deep learning methods to utilize visual perception information for predicting the SE(3) pose to manipulate the articulated object. (2) ManipLLM: the state-of-the-art MLLM model for predicting the SE(3) pose to manipulate the articulated object. (3) Base model: our base model trained solely on D_o without any other chain-of-thought data like ManipLLM. (4) Ours-w/o pretrain: change our model to base model and do not use TTA module. (5) Ours-w/o pos, Ours-w/o rot: the former doesn't use the position correction module, and the latter doesn't use the rotation correction

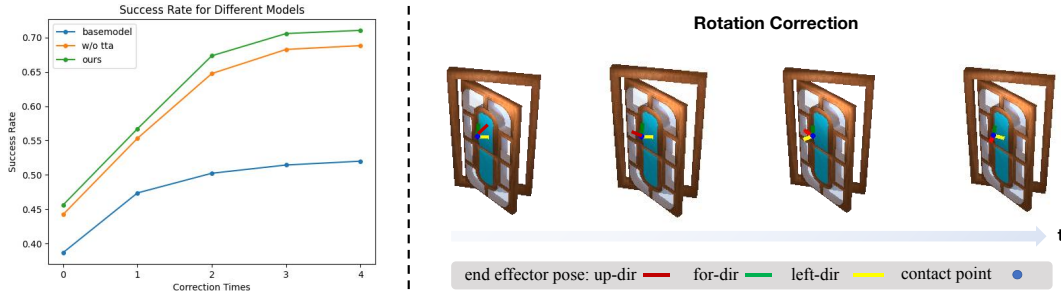


Figure 4: **Ablation of the proposed method and visualization.** The image on the left illustrates the correlation between success rate and correction times. On the right, the correction process is depicted with the aid of simulation.

module. Both of them do not use TTA module (6) Ours-w/o tta: Do not use the TTA module when testing (7) Ours: using four different types of data to train the MLLM to understand the prompt and applying AIC MLLM framework. For the settings from (4) to (7), we perform four corrections.

4.2 Main Results& Analysis

AIC MLLM can correct itself based on erroneous experiences, thereby achieving improved performance. Tab. 1 summarize all the experimental results. From the results, it is evident that our model shows significant improvement over the base model in both train and test categories. Moreover, with an increasing number of corrections (Fig. 4), the success rate progressively improves. This indicates that our model can correct itself based on failed experiences and continuously gather information and reflect on it to make further corrections as these experiences accumulate.

AIC MLLM makes the model more generalizable. Unlike other models, which show significant differences in performance between training and testing categories, our model achieves a success rate on testing categories 0.70 compared to that on training categories 0.72 (Tab. 1). This demonstrates the strong generalization capability of our framework, indicating that the information extracted pertains to the universal characteristics of articulated objects.

Train the model to understand the prompt is important. In Tab. 1, by comparing Ours-w/o pretrain and Ours-w/o TTA, we can see that training the model to understand interface prompts is crucial. This allows our model to improve from 57% to 69% on the train categories and from 45% to 68% on the test categories.

Contact point correction & rotation correction are both important. By comparing Ours-w/o pos, Ours-w/o rot, and Ours-w/o tta, we observe that using only rotation correction or only position correction results in a performance drop of approximately 10%. This demonstrates that both rotation and position corrections are essential, and their combined effect is crucial for our model to achieve optimal performance.

TTA is useful for AIC MLLM to adapt to the test domain By comparing Ours and Ours-w/o tta in Fig4, we find that the success rate of TTA at correction time 0 is higher than other settings, indicating that the TTA module enhances the model’s ability to perform manipulation tasks by learning from correction experiences. Additionally, from the final performance results, the inclusion of the TTA module effectively combats forgetting through learning rate decay. This leads to better performance in both train and test categories compared to ours-w/o TTA.

4.3 Real-world Experiment

After validating the effectiveness of our method in simulation, we conduct experiments in the real world. We use a Franka Emika robotic arm with a suction end effector and the D415 sensor to obtain RGB-D information. The detailed experimental setup and results can be found in supplement video.

5 Conclusion

We introduce AIC MLLM, a framework leveraging MLLM to correct SE(3) position predictions through learning from low-level interaction failures. We design visual and textual prompts for guiding position and rotation corrections, along with the integration of a feedback information extraction module to adaptively correct pose predictions based on identified failure causes. We implement test-time adaptation module to improve manipulation stability, with comprehensive experiments showcasing the effectiveness of AIC MLLM across simulated and real-world environments.

References

- [1] X. Zhu, D. Wang, O. Biza, G. Su, R. Walters, and R. Platt. Sample efficient grasp learning using equivariant models. *Proceedings of Robotics: Science and Systems (RSS)*, 2022.
- [2] H. Huang, D. Wang, X. Zhu, R. Walters, and R. Platt. Edge grasp network: A graph-based se (3)-invariant approach to grasp detection. *arXiv preprint arXiv:2211.00191*, 2022.
- [3] K. Zhou, L. Hong, C. Chen, H. Xu, C. Ye, Q. Hu, and Z. Li. Devnet: Self-supervised monocular depth learning via density volume construction. In *European Conference on Computer Vision*, pages 125–142. Springer, 2022.
- [4] K. Zhou. Neural surface reconstruction from sparse views using epipolar geometry. *arXiv e-prints*, pages arXiv–2406, 2024.
- [5] J. Zhang, J. Zhang, K. Pertsch, Z. Liu, X. Ren, M. Chang, S.-H. Sun, and J. J. Lim. Bootstrap your own skills: Learning to solve new tasks with large language model guidance. *arXiv preprint arXiv:2310.10021*, 2023.
- [6] R. Wang, J. Mao, J. Hsu, H. Zhao, J. Wu, and Y. Gao. Programmatically grounded, compositionally generalizable robotic manipulation. *arXiv preprint arXiv:2304.13826*, 2023.
- [7] S. Yang, J. Liu, R. Zhang, M. Pan, Z. Guo, X. Li, Z. Chen, P. Gao, Y. Guo, and S. Zhang. Lidar-llm: Exploring the potential of large language models for 3d lidar understanding. *arXiv preprint arXiv:2312.14074*, 2023.
- [8] J. Achiam, S. Adler, S. Agarwal, L. Ahmad, I. Akkaya, F. L. Aleman, D. Almeida, J. Altenschmidt, S. Altman, S. Anadkat, et al. Gpt-4 technical report. *arXiv preprint arXiv:2303.08774*, 2023.
- [9] J. Li, D. Li, S. Savarese, and S. Hoi. BLIP-2: Bootstrapping language-image pre-training with frozen image encoders and large language models, 2023.
- [10] H. Liu, C. Li, Q. Wu, and Y. J. Lee. Visual instruction tuning. *arXiv preprint arXiv:2304.08485*, 2023.
- [11] Z. Liu, A. Bahety, and S. Song. Reflect: Summarizing robot experiences for failure explanation and correction. *arXiv preprint arXiv:2306.15724*, 2023.
- [12] W. Huang, F. Xia, T. Xiao, H. Chan, J. Liang, P. Florence, A. Zeng, J. Tompson, I. Mordatch, Y. Chebotar, et al. Inner monologue: Embodied reasoning through planning with language models. *arXiv preprint arXiv:2207.05608*, 2022.
- [13] J. Liang, F. Xia, W. Yu, A. Zeng, M. G. Arenas, M. Attarian, M. Bauza, M. Bennice, A. Bewley, A. Dostmohamed, et al. Learning to learn faster from human feedback with language model predictive control. *arXiv preprint arXiv:2402.11450*, 2024.
- [14] C. Ming, J. Lin, P. Fong, H. Wang, X. Duan, and J. He. Hicrisp: A hierarchical closed-loop robotic intelligent self-correction planner. *arXiv preprint arXiv:2309.12089*, 2023.

- [15] L. Zha, Y. Cui, L.-H. Lin, M. Kwon, M. G. Arenas, A. Zeng, F. Xia, and D. Sadigh. Distilling and retrieving generalizable knowledge for robot manipulation via language corrections. *arXiv preprint arXiv:2311.10678*, 2023.
- [16] L. X. Shi, Z. Hu, T. Z. Zhao, A. Sharma, K. Pertsch, J. Luo, S. Levine, and C. Finn. Yell at your robot: Improving on-the-fly from language corrections. *arXiv preprint arXiv:2403.12910*, 2024.
- [17] Y. Guo, Y.-J. Wang, L. Zha, Z. Jiang, and J. Chen. Doremi: Grounding language model by detecting and recovering from plan-execution misalignment. *arXiv preprint arXiv:2307.00329*, 2023.
- [18] M. Skreta, N. Yoshikawa, S. Arellano-Rubach, Z. Ji, L. B. Kristensen, K. Darvish, A. Aspuru-Guzik, F. Shkurti, and A. Garg. Errors are useful prompts: Instruction guided task programming with verifier-assisted iterative prompting. *arXiv preprint arXiv:2303.14100*, 2023.
- [19] J. Liu, C. Li, G. Wang, L. Lee, K. Zhou, S. Chen, C. Xiong, J. Ge, R. Zhang, and S. Zhang. Self-corrected multimodal large language model for end-to-end robot manipulation. *arXiv preprint arXiv:2405.17418*, 2024.
- [20] W. Lin, X. Wei, R. An, P. Gao, B. Zou, Y. Luo, S. Huang, S. Zhang, and H. Li. Draw-and-understand: Leveraging visual prompts to enable mllms to comprehend what you want. *arXiv preprint arXiv:2403.20271*, 2024.
- [21] M. Cai, H. Liu, S. K. Mustikovela, G. P. Meyer, Y. Chai, D. Park, and Y. J. Lee. Making large multimodal models understand arbitrary visual prompts. *arXiv preprint arXiv:2312.00784*, 2023.
- [22] J. Yang, H. Zhang, F. Li, X. Zou, C. Li, and J. Gao. Set-of-mark prompting unleashes extraordinary visual grounding in gpt-4v. *arXiv preprint arXiv:2310.11441*, 2023.
- [23] X. Lei, Z. Yang, X. Chen, P. Li, and Y. Liu. Scaffolding coordinates to promote vision-language coordination in large multi-modal models. *arXiv preprint arXiv:2402.12058*, 2024.
- [24] D. Driess, F. Xia, M. S. Sajjadi, C. Lynch, A. Chowdhery, B. Ichter, A. Wahid, J. Tompson, Q. Vuong, T. Yu, et al. Palm-e: An embodied multimodal language model. *arXiv preprint arXiv:2303.03378*, 2023.
- [25] W. Huang, C. Wang, R. Zhang, Y. Li, J. Wu, and L. Fei-Fei. Voxposer: Composable 3d value maps for robotic manipulation with language models. *arXiv preprint arXiv:2307.05973*, 2023.
- [26] H. Geng, S. Wei, C. Deng, B. Shen, H. Wang, and L. Guibas. Sage: Bridging semantic and actionable parts for generalizable articulated-object manipulation under language instructions. *arXiv preprint arXiv:2312.01307*, 2023.
- [27] A. Brohan, N. Brown, J. Carbajal, Y. Chebotar, X. Chen, K. Choromanski, T. Ding, D. Driess, A. Dubey, C. Finn, et al. Rt-2: Vision-language-action models transfer web knowledge to robotic control. *arXiv preprint arXiv:2307.15818*, 2023.
- [28] X. Li, M. Zhang, Y. Geng, H. Geng, Y. Long, Y. Shen, R. Zhang, J. Liu, and H. Dong. Manipllm: Embodied multimodal large language model for object-centric robotic manipulation. *arXiv preprint arXiv:2312.16217*, 2023.
- [29] M. Cai, H. Liu, S. K. Mustikovela, G. P. Meyer, Y. Chai, D. Park, and Y. J. Lee. Making large multimodal models understand arbitrary visual prompts. In *IEEE Conference on Computer Vision and Pattern Recognition*, 2024.
- [30] A. Kirillov, E. Mintun, N. Ravi, H. Mao, C. Rolland, L. Gustafson, T. Xiao, S. Whitehead, A. C. Berg, W.-Y. Lo, P. Dollár, and R. Girshick. Segment anything. *arXiv:2304.02643*, 2023.

- [31] J. Wei, X. Wang, D. Schuurmans, M. Bosma, F. Xia, E. Chi, Q. V. Le, D. Zhou, et al. Chain-of-thought prompting elicits reasoning in large language models. *Advances in neural information processing systems*, 35:24824–24837, 2022.
- [32] Z. Xu, Z. He, and S. Song. Universal manipulation policy network for articulated objects. *IEEE robotics and automation letters*, 7(2):2447–2454, 2022.
- [33] B. Eisner, H. Zhang, and D. Held. Flowbot3d: Learning 3d articulation flow to manipulate articulated objects. *arXiv preprint arXiv:2205.04382*, 2022.
- [34] F. Xiang, Y. Qin, K. Mo, Y. Xia, H. Zhu, F. Liu, M. Liu, H. Jiang, Y. Yuan, H. Wang, L. Yi, A. X. Chang, L. J. Guibas, and H. Su. SAPIEN: A simulated part-based interactive environment. In *The IEEE Conference on Computer Vision and Pattern Recognition (CVPR)*, June 2020.
- [35] K. Mo, S. Zhu, A. X. Chang, L. Yi, S. Tripathi, L. J. Guibas, and H. Su. PartNet: A large-scale benchmark for fine-grained and hierarchical part-level 3D object understanding. In *The IEEE Conference on Computer Vision and Pattern Recognition (CVPR)*, June 2019.
- [36] R. Zhang, J. Han, A. Zhou, X. Hu, S. Yan, P. Lu, H. Li, P. Gao, and Y. Qiao. Llama-adaptor: Efficient fine-tuning of language models with zero-init attention. *arXiv preprint arXiv:2303.16199*, 2023.
- [37] A. Radford, J. W. Kim, C. Hallacy, A. Ramesh, G. Goh, S. Agarwal, G. Sastry, A. Askell, P. Mishkin, J. Clark, et al. Learning transferable visual models from natural language supervision. In *International conference on machine learning*, pages 8748–8763. PMLR, 2021.
- [38] H. Touvron, T. Lavril, G. Izacard, X. Martinet, M.-A. Lachaux, T. Lacroix, B. Rozière, N. Goyal, E. Hambro, F. Azhar, et al. Llama: Open and efficient foundation language models. *arXiv preprint arXiv:2302.13971*, 2023.
- [39] O. M. Andrychowicz, B. Baker, M. Chociej, R. Jozefowicz, B. McGrew, J. Pachocki, A. Petron, M. Plappert, G. Powell, A. Ray, et al. Learning dexterous in-hand manipulation. *The International Journal of Robotics Research*, 39(1):3–20, 2020.
- [40] W. Wan, H. Geng, Y. Liu, Z. Shan, Y. Yang, L. Yi, and H. Wang. Unidexgrasp++: Improving dexterous grasping policy learning via geometry-aware curriculum and iterative generalist-specialist learning. In *Proceedings of the IEEE/CVF International Conference on Computer Vision*, pages 3891–3902, 2023.
- [41] B. Huang, Y. Chen, T. Wang, Y. Qin, Y. Yang, N. Atanasov, and X. Wang. Dynamic handover: Throw and catch with bimanual hands. *arXiv preprint arXiv:2309.05655*, 2023.
- [42] H. Geng, Z. Li, Y. Geng, J. Chen, H. Dong, and H. Wang. Partmanip: Learning cross-category generalizable part manipulation policy from point cloud observations. In *Proceedings of the IEEE/CVF Conference on Computer Vision and Pattern Recognition*, pages 2978–2988, 2023.
- [43] T. Z. Zhao, V. Kumar, S. Levine, and C. Finn. Learning fine-grained bimanual manipulation with low-cost hardware. *arXiv preprint arXiv:2304.13705*, 2023.
- [44] C. Chi, S. Feng, Y. Du, Z. Xu, E. Cousineau, B. Burchfiel, and S. Song. Diffusion policy: Visuomotor policy learning via action diffusion. *arXiv preprint arXiv:2303.04137*, 2023.
- [45] K. Zhou, L. Hong, E. Xie, Y. Yang, Z. Li, and W. Zhang. Serf: Fine-grained interactive 3d segmentation and editing with radiance fields. *arXiv preprint arXiv:2312.15856*, 2023.
- [46] K. Mo, L. J. Guibas, M. Mukadam, A. Gupta, and S. Tulsiani. Where2act: From pixels to actions for articulated 3d objects. In *Proceedings of the IEEE/CVF International Conference on Computer Vision*, pages 6813–6823, 2021.

- [47] H. Zhang, B. Eisner, and D. Held. Flowbot++: Learning generalized articulated objects manipulation via articulation projection. *arXiv preprint arXiv:2306.12893*, 2023.
- [48] W. Dai, J. Li, D. Li, A. M. H. Tiong, J. Zhao, W. Wang, B. Li, P. N. Fung, and S. Hoi. Instructblip: Towards general-purpose vision-language models with instruction tuning. *Advances in Neural Information Processing Systems*, 36, 2024.
- [49] J. Li, D. Li, C. Xiong, and S. Hoi. Blip: Bootstrapping language-image pre-training for unified vision-language understanding and generation. In *International conference on machine learning*, pages 12888–12900. PMLR, 2022.
- [50] H. Liu, C. Li, Q. Wu, and Y. J. Lee. Visual instruction tuning. In *NeurIPS*, 2023.
- [51] Z. Yang, L. Li, K. Lin, J. Wang, C.-C. Lin, Z. Liu, and L. Wang. The dawn of lmms: Preliminary explorations with gpt-4v (ision). *arXiv preprint arXiv:2309.17421*, 9(1):1, 2023.

Appendix

A More related works.

Robotic Manipulation. Reinforcement learning[39, 40, 41, 42], imitation learning[43, 44, 45], and deep learning for visual understanding[46, 33, 47, 32] have been extensively applied in robotic manipulation. Recent studies like where2act[46] and Flowbot3d[33] combine prior knowledge with deep learning. Where2act[46] leverages point cloud data as input to initially predict the score of each point, followed by rotation prediction. UMPNet[32] employs a position network for position inference, then utilizes a action sampler to sample some directions of this position, and subsequently employs two networks to evaluate these directions. Flowbot3D[33] introduces an articulation flow to represent the point-wise potential motion and uses this representation to guide the manipulation. Flowbot++[47] integrates joint axis modeling into Flowbot3D to make the trajectory more smooth. Following the emergence of powerful large language models, researchers have started employing them to address the generalization challenges in manipulation tasks. Our work also focuses on leveraging large-scale models to enhance the robustness of algorithm in manipulation task.

Multimodal Large Language Models(MLLM). Large language models(LLM) have impressive power in natural language processing tasks. Consequently, some researchers aim to develop even more powerful MLLMs based on LLMs to tackle a broader range of vision-language tasks[48, 49, 9, 37, 36, 50]. CLIP[37] first established a connection between language and vision. The BLIP series[48, 49, 9] freezes the LLM and the image encoder, training their bridge, Q-Former, to align the two modalities. It also employs instruction tuning to enhance its ability to follow instructions. LLaVA[50] use a simple fully connected layer to build the bridge of the LLM and the image encoder. LLaMa-Adapter[36] utilizes projection and adapters to make the model have the multimodal ability and reduce training costs. Additionally, closed-source MLLMs like GPT-4V[51] are more powerful than the open-source models we mentioned previously.

B Detailed about Methodology and Implementation.

B.1 Rotation-related Information Extraction

In this section, we will provide a detailed introduction to how we perform joint type classification. After the end effector (EE) reaches the predicted pose and adheres to the object, it will move along the predicted gripper direction for a certain distance. We will record the pose trajectory of EE for 20 frames during this process. We denoted the i -th pose in the trajectory as ${}^W P_i^E$. We perform the operation of subtracting the previous pose from the current pose for all poses in the sequence which can be denoted as $\vec{v} = {}^W P_i^E - {}^W P_{i-1}^E$. We gather the \vec{v} to form a vector list. Then we calculate the angle between adjacent vectors. Next, we set a threshold. If all the angles are less than this threshold, then the joint will be considered a prismatic joint; otherwise, it will be considered a revolute joint.

















B.2 More Implementation Details















In this section, we will include additional implementation details that were not mentioned in the main paper. During the training phase, for the VQA task 'Mask Position Reasoning,' we mentioned that we randomly select N points. In implementation, N is set to 20. During testing, it is important to note that all MLLM temperatures are set to 0. In the tta training process, we initialize the learning rate(lr) to $5e-8$ and set the weight decay to $2e-3$. Every 300 iterations, we reduce the lr by 70%.

C More Ablation

Tab. 2 presents the ablation study results comparing the Vip-llava method and the GT method. Vip-llava uses the Vip-llava model to predict part mobility, while GT uses the ground truth interaction map. Across various categories, Vip-llava has some performance loss compared to GT, with average scores of 0.69 and 0.68 for training and test categories, respectively, compared to GT’s higher averages of 0.76 and 0.76. This indicates that Vip-llava’s understanding of embodied data is insufficient. Utilizing models with better comprehension of embodied data or incorporating human feedback into our framework could lead to improved results.

Table 2: Ablation study

Method	Train Categories															
																
Vip-llava	0.86	0.73	0.50	0.25	0.81	0.80	0.68	0.62	0.38	0.68	1.00	0.86	0.55	0.83	0.38	0.93
GT	0.81	0.78	0.75	0.78	0.81	0.67	0.86	0.85	0.44	0.79	1.00	0.75	0.74	0.83	0.38	0.73

Method	Train Categories					Test Categories										
					AVG											AVG
Vip-llava	0.60	0.70	0.27	1.00	0.69	0.36	0.45	0.76	0.83	0.64	0.86	0.70	0.78	0.64	0.69	0.68
GT	0.40	0.80	0.66	1.00	0.76	0.55	0.79	0.77	0.33	0.36	0.92	0.43	0.71	0.79	0.94	0.76

D Example of Prompts.

D.1 Position correction prompt

Firstly, we make use of the mask information to help the MLLM get a more precision prediction by the following prompts.

Is there a red mask in the image?	AIC-MLLM: No.
Is there a red mask in the image?	AIC-MLLM: Yes.

Determine if following point is in the red mask: (172,47),(117,192),(323,251),(195,9),(211,277),(242,292),(87,70),(88,314),(193,39),(87,174),(88,165),(25,333),(72,265),(115,243),(197,335),(99,177),(243,285),(147,147),(288,265),(185,127)	AIC-MLLM: No,Yes,No,No,No,No,No,No,No,No,No,No,No,No,Yes,No,No,No,Yes,No,Yes
Determine if following point is in the red mask: (11,104),(212,138),(182,125),(156,111),(258,27),(217,151),(309,307),(174,148),(29,67),(35,295),(73,297),(302,218),(259,287),(265,27),(199,61),(44,290),(88,33),(133,232),(255,36),(256,290)	AIC-MLLM: No,No,Yes,Yes,Yes,No,No,Yes,No,No,No,No,No,No,No,Yes,No,No

For position correction using the red mask image, we reassess the validity of the previously predicted contact point. If the contact point is deemed ideal, the MLLM will confirm this by replying "Yes." Otherwise, it will reply "No."

Given the part with a red mask known to be unmovable in the image, is the (112,171) considered as the successful contact point?	AIC-MLLM: Yes.
Given the part with a red mask known to be unmovable in the image, is the (160,160) considered as the successful contact point?	AIC-MLLM: No.

Then, MLLM makes the prediction using the image with red mask.

Specify the successful contact point and orientation of pulling the object. DONOT predict the successful contact point in the red mask part.
AIC-MLLM: The contact point is at (170, 179), the gripper direction is [48, -1, -12], the gripper forward direction is [-1, 1, 49].
Specify the successful contact point and orientation of pulling the object. DONOT predict the successful contact point in the red mask part.
AIC-MLLM: The contact point is at (143, 174), the gripper direction is [48, 1, 12], the gripper forward direction is [1, -49, -10].

MLLM assesses whether the predicted point is a successful point.

You pull the object in the picture by point(170,162),gripper direction[47,11,-11],gripper forward direction[10,-49,1],if it will success answer only Yes , else answer only No.
AIC-MLLM: No.
You pull the object in the picture by point(179,179),gripper direction[38,-28,13],gripper forward direction[13,45,-19],if it will success answer only Yes , else answer only No.
AIC-MLLM: Yes.

D.2 Rotation correction prompt

The FIE acquires environmental information, including joint type, joint axis and the normal direction of previously predicted contact point. The MLLM uses this information, along with the contact point, to infer whether to correct its response by suggesting a new gripper direction.

You're trying to pull an object part, the joint's type is REVOLUTE, the joint axis direction is [-22, -1, 44]. Your contact point is (79, 170), the norm direction of the point is [-47, 9, 12]. Please tell me your gripper direction.
AIC-MLLM: The gripper direction is [-47, 13, -13].
You're trying to pull an object part, the joint's type is REVOLUTE, the joint axis direction is [10, 6, -48]. Your contact point is (170, 159), the norm direction of the point is [-29, 0, 40].Please tell me your gripper direction.
AIC-MLLM: The gripper direction is [-28, 35, -20].

E Example of Failed Case and correction process.

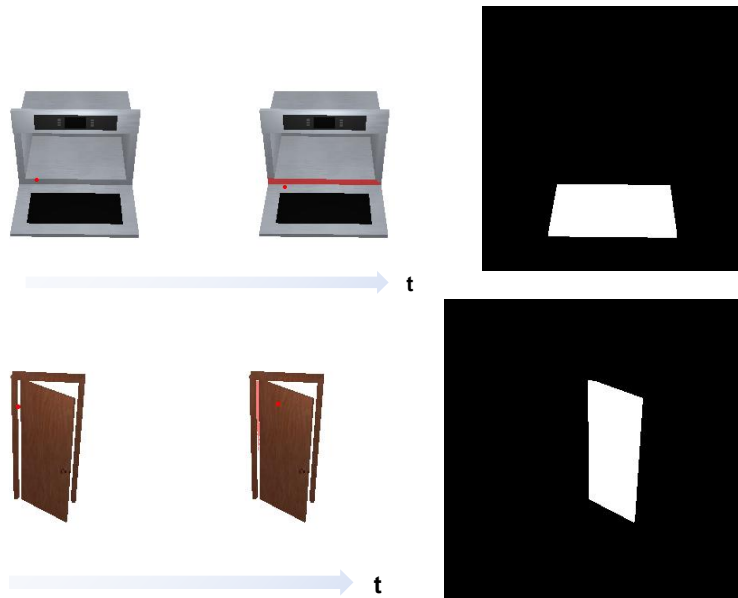


Figure 5: **Examples of position correction.** The first figure is the original prediction of contact point, and the red dot in the second figure is a new prediction of contact point keeping away from the red mask. And the third figure is the interaction map where white area is the movable part of the object.



Figure 6: **Rotation correction.** Correction times increase sequentially along the timeline.

F Real-world experiments

To validate our end-to-end method beyond simulations, we conducted real-world experiments using a Franka Emika robotic arm equipped with an Intel RealSense D415 sensor. For more details, please refer to the video and our website (<https://sites.google.com/view/aic-ml1m>).

Experimental Setup. The setup included a Franka Emika Panda robotic arm, known for its precision and versatility. An Intel RealSense D415 sensor was used to capture RGB-D data, providing

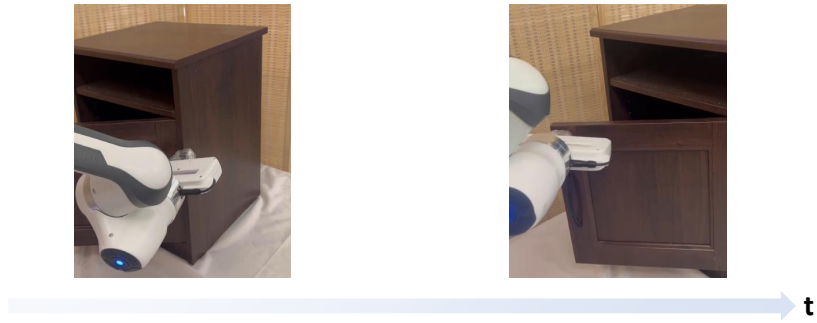


Figure 7: **Real-world experiment.** Correction times increase sequentially along the timeline. The left figure shows a failed prediction, while the right figure shows a successful prediction corrected by our AIC MLLM.

3D information necessary for the robotic arm’s operations. We closed the traditional gripper and applied double-sided tape to its head as a suction gripper.

Initialization. The robotic arm and D415 sensor were calibrated to ensure accurate spatial data capture and precise movements.

Image Processing. The D415 sensor captures high-resolution RGB-D images, which are processed to meet the requirements of our pipeline. Specifically, our method necessitates images sized at 336x336 pixels. To preserve information during resizing, we apply both cropping and padding techniques. This involves cropping or adding white borders around the captured images to resize them to 336x336 pixels. The resulting image, whether cropped or padded, is then used for further analysis in our end-to-end pipeline.

Task Execution. Using our end-to-end method, the robotic arm was directly controlled to perform tasks based on the RGB-D data input. The tasks involved the arm autonomously approaching and manipulating objects within the workspace.

Demonstration. The robotic arm demonstrated its ability to perform these tasks seamlessly, showcasing the practical applicability and robustness of our end-to-end method in handling real-world scenarios.